

## Monometallic Catalytic Models Hosted in Stable Metal-Organic Frameworks for Tunable CO<sub>2</sub> Photoreduction

Xiao-Kun Wang, jiang liu, Lei Zhang, Long-Zhang Dong, Shun-Li Li, Yu-He Kan, Dongsheng Li, and Ya-Qian Lan

*ACS Catal.*, **Just Accepted Manuscript** • DOI: 10.1021/acscatal.8b04887 • Publication Date (Web): 15 Jan 2019

Downloaded from <http://pubs.acs.org> on January 16, 2019

### Just Accepted

“Just Accepted” manuscripts have been peer-reviewed and accepted for publication. They are posted online prior to technical editing, formatting for publication and author proofing. The American Chemical Society provides “Just Accepted” as a service to the research community to expedite the dissemination of scientific material as soon as possible after acceptance. “Just Accepted” manuscripts appear in full in PDF format accompanied by an HTML abstract. “Just Accepted” manuscripts have been fully peer reviewed, but should not be considered the official version of record. They are citable by the Digital Object Identifier (DOI®). “Just Accepted” is an optional service offered to authors. Therefore, the “Just Accepted” Web site may not include all articles that will be published in the journal. After a manuscript is technically edited and formatted, it will be removed from the “Just Accepted” Web site and published as an ASAP article. Note that technical editing may introduce minor changes to the manuscript text and/or graphics which could affect content, and all legal disclaimers and ethical guidelines that apply to the journal pertain. ACS cannot be held responsible for errors or consequences arising from the use of information contained in these “Just Accepted” manuscripts.



# Monometallic Catalytic Models Hosted in Stable Metal-Organic Frameworks for Tunable CO<sub>2</sub> Photoreduction

Xiao-Kun Wang<sup>†a</sup>, Jiang Liu<sup>†b</sup>, Lei Zhang<sup>b</sup>, Long-Zhang Dong<sup>b</sup>, Shun-Li Li<sup>b</sup>, Yu-He Kan<sup>c</sup>, Dong-Sheng Li<sup>\*a</sup>, Ya-Qian Lan<sup>\*b</sup>

[a] College of Materials and Chemical Engineering, Key Laboratory of Inorganic Nonmetallic Crystalline and Energy Conversion Materials, China Three Gorges University, No. 8, Daxue Road, Yichang, 443002, P. R. China

[b] School of Chemistry and Materials Science, Jiangsu Key Laboratory of Biofunctional Materials, Nanjing Normal University, Nanjing 210023, P. R. China

[c] Jiangsu Province Key Laboratory for Chemistry of Low-Dimensional Materials, School of Chemistry and Chemical Engineering, Huaiyin Normal University, Huaian 223300, P.R. China

**ABSTRACT:** The photocatalytic reduction of CO<sub>2</sub> to energy carriers has emerged as one of the most promising strategy to alleviate the energy crisis and CO<sub>2</sub> pollution, for which the development of catalyst was considered as the determining factor for the accomplishment of this conversion process. In this study, three stably and isostructural metal organic frameworks (denoted as **MOF-Ni**, **MOF-Co** and **MOF-Cu**), have been synthesized and used as heterogeneous catalysts applied into photocatalytic CO<sub>2</sub> reduction reaction (CO<sub>2</sub>RR). It is worth noting that the **MOF-Ni** exhibited a very high selectivity of 97.7% for photoreducing CO<sub>2</sub> to CO, which has exceeded most of the reported MOF-based catalysts in the field. Significantly, the MOFs associated with monometallic catalytic centre offer a simply and precisely structural model which allows us to understand the specific effects of different metal ion species on photoreduction of CO<sub>2</sub> as well as reactive mechanism more intuitively.

**KEYWORDS:** *Metal-Organic Frameworks, Isostructural, Photocatalytic CO<sub>2</sub> Reduction, High Selectivity, Monometallic Catalytic Model, Reactive Mechanism*

In recent years, the increased emission of anthropogenic CO<sub>2</sub> from the burning of fossil fuels is leading to serious issues such as global warming and energy crisis. Great efforts in finding efficient strategies to solve these problems have been made.<sup>1-2</sup> For instance, considering that solar energy is a clean and renewable energy source, visible-light driven photocatalytic CO<sub>2</sub>RR that converting CO<sub>2</sub> into carbon-based energy carriers (hydrocarbon fuels or chemicals) has been considered as one of the most promising solutions.<sup>3-6</sup> However, the difficult activation process of CO<sub>2</sub> molecule with intrinsically chemical inertness enables the reaction to undergoing large thermodynamic barriers. Fortunately, the development of efficient and selective catalysts has been proven to be extremely vital in addressing above issue. Up to now, a variety of semiconductors (e.g., TiO<sub>2</sub>, ZrO<sub>2</sub>, Bi<sub>2</sub>WO<sub>6</sub> and WO<sub>3</sub>) and nanocomposites have been used as photocatalysts to exert CO<sub>2</sub>RR.<sup>7-11</sup> Although most semiconductor-based nanomaterials exhibit high photocatalytic performance, the complicated structural components and indistinct active sites are always difficult to productive in investigating the reactive mechanism.<sup>12-15</sup> Consequently, how to develop an efficient photocatalyst with precisely structural information in principle is the important prerequisite for the explanation of photocatalytic mechanism of CO<sub>2</sub>RR.<sup>16</sup>

Metal-organic framework (MOF) constructed by metal ions/clusters and functionalized organic ligands is one kind of crystalline material with well-defined structure. Because of the structural tailorability and ultrahigh surface area, MOF has been applied in many fields widely.<sup>17-31</sup> Recently, many studies have demonstrated that MOFs can serve as catalysts to reduce CO<sub>2</sub> as well as offer a good platform to study reaction mechanism from molecular level, and the research heat of this study continues to increase.<sup>32-41</sup> However, the reaction condition of CO<sub>2</sub>

photoreduction is somewhat harsh that commonly requires the catalyst that has highly structural stability in reaction solution. This is actually a big challenge to the majority of the reported crystalline MOF. In particular, the CO<sub>2</sub>RR carried out in relatively alkaline system, which is beneficial for the dissolution of more CO<sub>2</sub>, has additional requirements on the chemical stability of involved MOF. Additionally, the active centers of most MOF-based catalysts are mainly homo-/hetero-metallic cluster as secondary building units (SBUs).<sup>42-44</sup> Due to the collaborative contribution and interaction between active centres within cluster on the photocatalytic performance, the catalytic ability of single metal active site is hard to evaluate such that the relevant reaction mechanism is still elusive and intricate.<sup>45-47</sup> Consequently, the construction of MOF-based catalyst with single catalytic active center and high structural robustness to overcome the aforementioned troubles is supposed to be desirable.

With these considerations in mind, we successfully designed and synthesized three stable and isomorphous MOFs, {Cu<sub>3</sub>(TCA)<sub>2</sub>(dpe)<sub>3</sub>(H<sub>2</sub>O)<sub>3</sub>}<sub>n</sub> (**MOF-Cu**), {Co<sub>3</sub>(TCA)<sub>2</sub>(dpe)<sub>3</sub>(H<sub>2</sub>O)<sub>6</sub>}<sub>n</sub> (**MOF-Co**) and {Ni<sub>3</sub>(TCA)<sub>2</sub>(dpe)<sub>3</sub>(H<sub>2</sub>O)<sub>6</sub>}<sub>n</sub> (**MOF-Ni**), which are used different transition metal centers (Cu<sup>II</sup>, Co<sup>II</sup> and Ni<sup>II</sup>) and mixed organic ligands [4,4',4''-nitrilotribenzoic acid ligands (TCA) and 1,2-di (4-pyridyl) ethylene (dpe)]. It is noteworthy that these MOFs use single active metal centre as node which implies a simple and straightforward structural model to analyze the influence of different transition metal centres on photocatalytic reduction of CO<sub>2</sub>. As expected, the MOFs with different catalytic active centres (Cu<sup>II</sup>, Co<sup>II</sup> and Ni<sup>II</sup>) were treated as catalysts applied in heterogeneous photocatalytic CO<sub>2</sub>RR, which indeed resulted in notable effects on the sort and selectivity of mainly reductive products. Interestingly, **MOF-Ni** exhibited very high catalytic

selectivity (97.7%) of CO, which has surpassed most of the reported MOF-based catalysts applied in photocatalytic CO<sub>2</sub>RR, representing the most efficient MOF-based catalyst with Ni<sup>II</sup> ion as active centre. By contrast, **MOF-Cu** and **MOF-Co** showed high selectivity (77.4%) of H<sub>2</sub> and moderate selectivity (47.4%) of CO, respectively. Notably, the corresponding theoretical calculations are consistent with the photocatalytic prosperities and offer an important insight into the influence of different monometallic catalytic centres on photocatalytic CO<sub>2</sub> conversion.

Single-crystal X-ray diffraction analysis reveals that **MOF-Cu**, **MOF-Co** and **MOF-Ni** have almost identical host framework, all of them crystallize in the trigonal system with R-3 space group. The only difference is that five-coordinated Cu<sup>II</sup> ion adopts tetragonal pyramid geometry, while Co<sup>II</sup> and Ni<sup>II</sup> ions have one more axial coordination H<sub>2</sub>O molecule to form an octahedron environment (Figure 1a, S1, S2). The coordination sphere of Cu<sup>II</sup> ion is surrounded by two carboxylate-O atoms from two TCA ligands, two N atoms from two dpe ligands and one O atom from axial coordination H<sub>2</sub>O molecule. Considering that **MOF-Co** and **MOF-Ni** are isomorphic, **MOF-Ni** is selected to describe their structures herein. **MOF-Co** and **MOF-Ni** embrace equivalent two couples of N and O atoms as same as Cu<sup>II</sup> ion in equatorial plane and two O atoms from two axial coordination H<sub>2</sub>O molecules. The Ni-N/O bond lengths in equatorial plane are in the range of 2.0-2.1 Å, while the axial Ni-O bond lengths are 2.0 Å.<sup>48-50</sup> The carboxylate group of TCA ligand adopts a μ<sup>1-η</sup>:η<sup>0</sup> coordination mode and each TCA ligand connect three different Ni<sup>II</sup> ions (Figure S3a). Notably, TCA ligands are connected with Ni ions along the crystallographic *c* axis to form 2D network having a twisted hexagon window (Figure S3b), and 2D networks are three-fold interpenetrated into a layered structure (Figure 1b). Interestingly, the adjacent 2D layers are further pillared by the dpe ligands to form an overall 3D network (Figure 1c and S4). Additionally, the framework of **MOF-Ni** and **MOF-Co** can be described as 3,4-connected networks with the Schläfli symbol {10<sup>3</sup>}<sub>2</sub>{10<sup>6</sup>}<sub>3</sub> from topology (Figure S5).

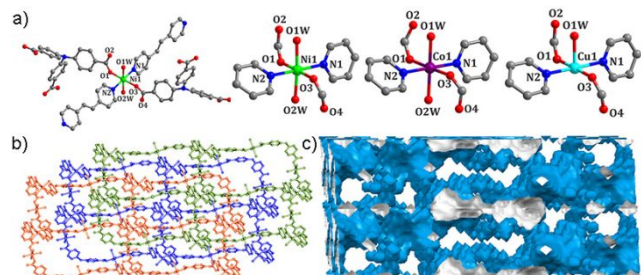


**Figure 1.** (a) Coordination environment of MOFs. (b) Schematic view of the three-fold interpenetrating layer. (c) 3D channel simulated diagram of **MOF-Ni**.

The purity of the as-synthesized crystals was verified by powder X-ray diffraction (PXRD) pattern which showed well match with the simulated one from crystal structure (Figure 2a, S7, S8). It is found that these MOFs exhibit good chemical stabilities that can keep their structures unchanged under broad pH value variation ranges. Furthermore, their high thermal stabilities were also verified by the thermogravimetric (TG) curves under O<sub>2</sub> flow (Figure S9).

The UV/vis spectra demonstrate that these three isostructural MOFs show very broad absorption throughout the region of 450-800 nm, indicating their potential to be catalyst applied to photocatalysis (Figure 2b). In order to clarify the semiconductor properties of these MOFs and the possibility of subsequent photoreduction of CO<sub>2</sub>, Mott-Schottky measurements were performed at frequencies of 500, 1000 and 1500 Hz. The results indicate that these three MOFs are typical n-type semiconductors (Figure 2c, and Figure S10, S11). Since the intersection point is

independent of the frequency, the flat positions of **MOF-Ni**, **MOF-Co** and **MOF-Cu** are determined to be -1.14, -1.34 and -1.28 V vs Ag/AgCl, respectively. Thus the bottom of the conduction band (LUMO) of **MOF-Ni**, **MOF-Co** and **MOF-Cu** are estimated to be -0.94, -1.14 and -1.08 V vs the normal hydrogen electrode (NHE), respectively.<sup>51</sup> From the Tauc plot, the bandgaps of the **MOF-Ni**, **MOF-Co** and **MOF-Cu** were estimated to be 1.50, 2.02 and 1.77 eV by Kubelka-Munk (KM) method (Figure S12, S13, S14). Then the valence band (HOMO) positions of these three MOFs were calculated to be 0.56, 0.88 and 0.69 eV versus NHE, respectively. Since their LUMO positions are more negative than the reduction potentials of CO<sub>2</sub> to many products, it is theoretically feasible to use these MOFs as catalysts for photoreducing CO<sub>2</sub>.<sup>12, 52</sup> Additionally, the adsorption of CO<sub>2</sub> is often believed to play a crucial role in the catalytic performance of catalyst, so the volumetric CO<sub>2</sub> adsorption measurements were performed on the activated samples at 298 K.<sup>53-54</sup> As shown in Figure 2d, the CO<sub>2</sub> uptakes at 298K were found to be 40.35, 38.87, 34.00 cm<sup>3</sup> g<sup>-1</sup> for **MOF-Co**, **MOF-Ni** and **MOF-Cu**, respectively.

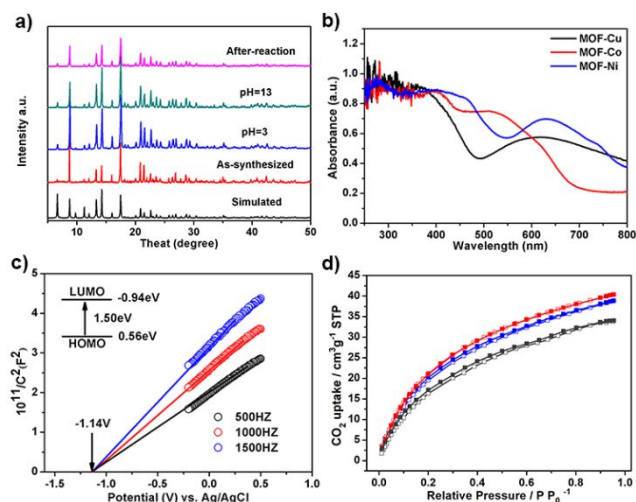


**Figure 2.** (a) PXRD patterns of **MOF-Ni**. (b) The UV-vis spectra of **MOF-Ni** (blue), **MOF-Cu** (black) and **MOF-Co** (red). (c) Mott-Schottky plots for **MOF-Ni** in 0.2 M Na<sub>2</sub>SO<sub>4</sub> aqueous solution. (d) CO<sub>2</sub> adsorption behavior for **MOF-Co** (red) as well as **MOF-Ni** (blue) and **MOF-Cu** (black) at 298 K.

Taking the above features of these MOFs into consideration, the photocatalytic CO<sub>2</sub>RR was conducted under a pure CO<sub>2</sub> (1.0 atm, 298 K) atmosphere in a mixed solution of MeCN/H<sub>2</sub>O (13:1) with triisopropanolamine (TIPA) as an electron donor. Besides, [Ru(bpy)<sub>3</sub>]Cl<sub>2</sub>·6H<sub>2</sub>O (bpy = 2,2'-bipyridine) as an auxiliary photosensitizer (PS) was added into the reaction system for increasing visible-light absorption.<sup>12, 55</sup> Because of the matched LUMO positions between the PS and MOF-based catalysts (Figure S15-S17), photo-generated electrons were allowed to migrate from the PS to the MOFs.<sup>56-57</sup> Based on the different optical and electrochemical properties of these isomorphic MOFs, their differences on the performance of CO<sub>2</sub>RR can be demonstrated through a series of photocatalytic experiments. As shown in Figure 3a, increasing the generation of CO (22.3 μmol, i.e., 371.6 μmol g<sup>-1</sup> h<sup>-1</sup>) rather than H<sub>2</sub> (0.5 μmol, i.e., 8.3 μmol g<sup>-1</sup> h<sup>-1</sup>) were observed when reducing CO<sub>2</sub> with **MOF-Ni** as a photocatalyst under visible light irradiation (λ ≥ 420 nm) (Figure 3b). By contrast, **MOF-Co** displayed a dramatic promotion on the production of CO (22.8 μmol, i.e., 1140.0 μmol g<sup>-1</sup> h<sup>-1</sup>) and H<sub>2</sub> (25.3 μmol, i.e., 1265.0 μmol g<sup>-1</sup> h<sup>-1</sup>), while only 1.7 μmol (i.e., 68.0 μmol g<sup>-1</sup> h<sup>-1</sup>) CO and 5.8 μmol (i.e., 232.0 μmol g<sup>-1</sup> h<sup>-1</sup>) H<sub>2</sub> by **MOF-Cu** at the same reaction system. The TONs of these photocatalytic systems were summarized in Table S3. Remarkably, the **MOF-Ni** exhibits a higher selectivity of CO over H<sub>2</sub> (97.7%) than **MOF-Co** (47.4%)

and **MOF-Cu** (22.6%). Furthermore, among the reported of heterogeneous MOF-based catalysts applied in the photocatalytic CO<sub>2</sub>RR that exhibited such a high selectivity towards CO have been rarely seen. Gaseous CO and H<sub>2</sub> were the main reaction products detected by gas chromatography during the whole photocatalytic process, only trace amounts of HCOOH were produced in the aqueous solution as detected by ion chromatography.

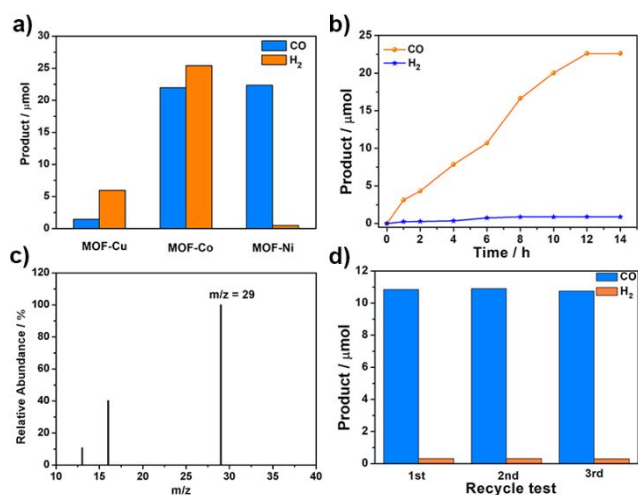


**Figure 3.** (a) Photocatalytic production of CO and H<sub>2</sub> catalyzed by **MOF-Cu**, **MOF-Co** and **MOF-Ni**. (b) A amount of CO and H<sub>2</sub> produced as a function of the time of visible-light irradiation over **MOF-Ni**. (c) Mass spectra ( $m/z=29$ ) analyse of the source of CO. (d) Average yields of CO and H<sub>2</sub> in fresh 7 h with **MOF-Ni** catalysts in recycling tests.

Considering that **MOF-Ni** has better catalytic activity and selectivity than **MOF-Cu** and **MOF-Co** in photocatalytic CO<sub>2</sub>RR, a series of reference experiments with **MOF-Ni** as the example were conducted to determine the importance role of the catalyst and the experimental results are summarized in the Table S3. The production of CO has a high selectivity of 97.7% over competing H<sub>2</sub> generation after 12 hours irradiation with visible light. This selectivity is the highest among most of the reported MOF-based photocatalysts for reducing CO<sub>2</sub> to CO (Table S4). The calculated quantum yield of the heterogeneous photocatalytic system was  $5.3 \times 10^{-3}\%$  under irradiation of 420 nm light (specific calculation method in the ESI). To ascertain the source of the produced CO, we performed an isotopic tracing experiment by replacing CO<sub>2</sub> with <sup>13</sup>CO<sub>2</sub>. The <sup>13</sup>CO<sub>2</sub> was used as the reactant under the same photocatalytic reaction condition, and then the reaction product was examined by gas chromatography-mass spectrometry. After irradiation with visible light, the peak at 1.8 min with  $m/z$  29 was assigned to <sup>13</sup>CO (Figure 3c). The results demonstrate that CO<sub>2</sub> is the main carbon source rather than the degradation of organics in the reaction. Additionally, the total production of the reaction products has no noticeable decrease after four cycles of 7 hours reaction, suggesting the reservation of the original photocatalytic activity of **MOF-Ni** (Figure 3d). Furthermore, there was no noticeable alteration in their PXRD patterns and IR spectra obtained before and after the photocatalytic reactions that evidenced the structural robustness of the catalyst again (Figure S23-S25).

To explore the reasons for the difference in photocatalytic activity of the three catalysts, we first assume that charge separation efficiency is an important factor.<sup>58</sup> As proved by the photocurrent characterization results, **MOF-Ni** and **MOF-Co** reveal obviously more efficient separation of photogenerated electron-hole pairs than **MOF-Cu** under the same conditions (Figure S26). The fact is further supported by electrochemical

impedance spectroscopy (EIS), which indicates that **MOF-Co** has the smallest radius and the lowest resistance in charge transportation, while **MOF-Cu** shows the biggest radius and the largest resistance among them (Figure S27). Therefore, **MOF-Co** and **MOF-Ni** possess higher charge-separation efficiency than **MOF-Cu**.

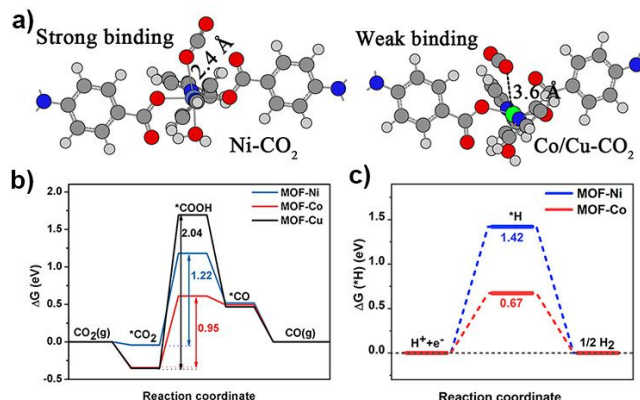


**Figure 4.** (a) Geometry structures of CO<sub>2</sub> adsorbed on three metal sites, the Ni is present as dark blue and Co/Cu are in green. (b) The free energy profile of CO<sub>2</sub>RR toward the production of CO. (c) The free energy diagram of HER.

Density functional theory (DFT) calculations are performed to understand the specific effects of different metal ion species on photoreduction of CO<sub>2</sub>. We first investigate the binding between CO<sub>2</sub> and three metal ions, which plays an essential role in the selectivity and reactivity of the following catalytic reactions. As shown in Figure 4a, both Co and Cu present weak interaction toward to CO<sub>2</sub> with a long distance of 3.6 Å, while Ni and CO<sub>2</sub> form strong coordination bond of 2.4 Å. The strong coupling between Ni and CO<sub>2</sub> is attributed to the high spin state of the Ni in an octahedral coordination, as seen in the spin density plot (Figure S30). However, the binding energy, calculated by  $E_{BE}(*CO_2) = E(\text{total}) - E(5\text{-coordination}) - E(CO_2)$ , is determined to be a small value due to the coupling between Ni and two O in the carboxyl group (Figure S31). Free energy pathways of CO<sub>2</sub> reduction to CO on the metal sites of MOFs and the intermediate structures are shown in Figure 4b and S32. Among the four elementary reaction steps, the \*COOH formation serves as the rate-limiting step and follows the order of Cu (2.04 eV) > Ni (1.22 eV) > Co (0.95 eV). The competition reaction of hydrogen evolution reaction (HER) is considered for comparison and the free energy diagram obtains 0.67 eV for Co and 1.42 eV for Ni respectively (Figure 4c). The calculation results suggest that **MOF-Ni** presents the best selectivity among the three complexes due to the strong binding with CO<sub>2</sub> and high HER free energy, and both CO<sub>2</sub>RR and HER processes can readily occur for **MOF-Co**. These findings are in good agreement with the aforementioned experiments.

In accordance with the above experimental results and theoretical calculations, a possible photocatalytic mechanism was proposed (Figure 5). First, the coordination water on the metal center is easily detached to form exposed metal active site, where CO<sub>2</sub> molecules are adsorbed. Since the LUMO of MOF-M is lower than that of [Ru(bpy)<sub>3</sub>]<sup>2+</sup>, the photo-generated electrons in the LUMO of [Ru(bpy)<sub>3</sub>]<sup>2+</sup> can be transferred to the surface of the MOF-M.<sup>59-60</sup> Second, the CO<sub>2</sub> adsorbed on the metal active site accepts an electron to form radical CO<sup>-</sup> intermediate. Third, by the proton-assisted two-electron transport process, the adsorbed CO<sub>2</sub> molecule was finally reduced to CO. Finally, the excited state of photosensitizer was reductive quenching by the sacrificial electron donor TIPA and the generated CO detached from the catalyst surface.

In summary, three isostructural and stable transition metal-based MOFs were synthesized and used as catalysts applied in the heterogeneous photocatalytic CO<sub>2</sub>RR. It is significant that MOF-Ni displays a very high selectivity of 97.7% for the CO<sub>2</sub>-to-CO conversion, which has surpassed most of the reported MOF-based catalysts in the field of CO<sub>2</sub>RR. Furthermore, the precisely and simply structural models with single metal active site enable us to understand the specific effects of different metal ion species on

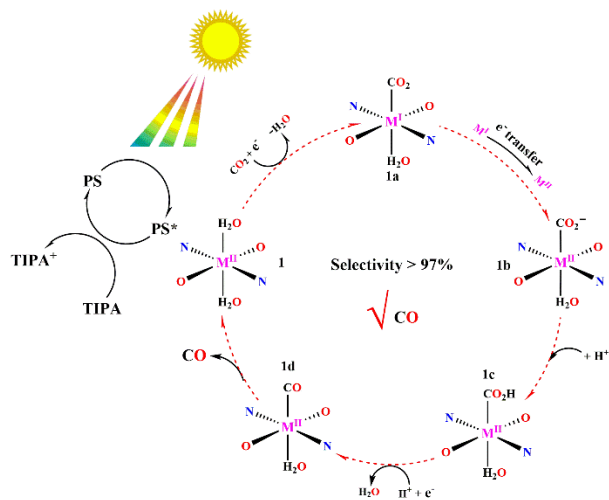


**Figure 5.** Proposed photocatalytic mechanism of MOFs for the CO<sub>2</sub> to CO conversion.

photoreduction of CO<sub>2</sub> and reactive mechanism more intuitively. Our findings are anticipated to providing more insights into the development of more efficient, stable and selective catalysts for photocatalytic CO<sub>2</sub>RR.

## AUTHOR INFORMATION

### Corresponding Author

\* E-mail addresses: [yqlan@njnu.edu.cn](mailto:yqlan@njnu.edu.cn), [lidongsheng1@126.com](mailto:lidongsheng1@126.com).

### Author Contributions

†These authors contributed equally.

### Notes

The authors declare no competing financial interest.

### Supporting Information

This material is available free of charge via the Internet at <http://pubs.acs.org>.

Crystallographic data for three MOFs.

Details of synthesis, more characterization, and theoretical calculations.

## ACKNOWLEDGMENT

This work was financially supported by NSF of China (21673127), and the 111 project of Hubei Province (2018-19).

## REFERENCES

- (1) Zhang, N.; Wang, L.; Wang, H.; Cao, R.; Wang, J.; Bai, F.; Fan, H. Self-Assembled One-Dimensional Porphyrin Nanostructures with Enhanced Photocatalytic Hydrogen Generation. *Nano Lett.* **2018**, *18*, 560-566.
- (2) Kim, W.; McClure, B. A.; Edri, E.; Frei, H. Coupling carbon dioxide reduction with water oxidation in nanoscale photocatalytic assemblies. *Chem. Soc. Rev.* **2016**, *45*, 3221-3243.
- (3) Listorti, A.; Durrant, J.; Barber, J. Artificial photosynthesis: solar to fuel. *Nat. Mater.* **2009**, *8*, 929.

- (4) Tu, W.; Zhou, Y.; Zou, Z. Photocatalytic conversion of CO<sub>2</sub> into renewable hydrocarbon fuels: state-of-the-art accomplishment, challenges, and prospects. *Adv. Mater.* **2014**, *26*, 4607-4626.
- (5) Zong, X.; Han, J.; Seger, B.; Chen, H.; Lu, G.; Li, C.; Wang, L. An integrated photoelectrochemical-chemical loop for solar-driven overall splitting of hydrogen sulfide. *Angew. Chem. Int. Ed.* **2014**, *53*, 4399-4403.
- (6) Diercks, C. S.; Liu, Y.; Cordova, K. E.; Yaghi, O. M. The role of reticular chemistry in the design of CO<sub>2</sub> reduction catalysts. *Nat. Mater.* **2018**, *17*, 301-307.
- (7) Habisreutinger, S. N.; Schmidt-Mende, L.; Stolarczyk, J. K. Photocatalytic reduction of CO<sub>2</sub> on TiO<sub>2</sub> and other semiconductors. *Angew. Chem. Int. Ed.* **2013**, *52*, 7372-7408.
- (8) Schneider, J.; Matsuoka, M.; Takeuchi, M.; Zhang, J.; Horiuchi, Y.; Anpo, M.; Bahnemann, D. W. Understanding TiO<sub>2</sub> photocatalysis: mechanisms and materials. *Chem. Rev.* **2014**, *114*, 9919-9986.
- (9) Xiao, F.-X.; Miao, J.; Liu, B. Layer-by-layer self-assembly of CdS quantum dots/graphene nanosheets hybrid films for photoelectrochemical and photocatalytic applications. *J. Am. Chem. Soc.* **2014**, *136*, 1559-1569.
- (10) Wu, J.; Li, X.; Shi, W.; Ling, P.; Sun, Y.; Jiao, X.; Gao, S.; Liang, L.; Xu, J.; Yan, W. Efficient Visible-Light-Driven CO<sub>2</sub> Reduction Mediated by Defect-Engineered BiOBr Atomic Layers. *Angew. Chem. Int. Ed.* **2018**, *57*, 8719-8723.
- (11) Gao, C.; Meng, Q.; Zhao, K.; Yin, H.; Wang, D.; Guo, J.; Zhao, S.; Chang, L.; He, M.; Li, Q. Co<sub>3</sub>O<sub>4</sub> Hexagonal Platelets with Controllable Facets Enabling Highly Efficient Visible-Light Photocatalytic Reduction of CO<sub>2</sub>. *Adv. Mater.* **2016**, *28*, 6485-6490.
- (12) Tong, H.; Ouyang, S.; Bi, Y.; Umezawa, N.; Oshikiri, M.; Ye, J. Nano-photocatalytic materials: possibilities and challenges. *Adv. Mater.* **2012**, *24*, 229-251.
- (13) Kuriki, R.; Sekizawa, K.; Ishitani, O.; Maeda, K. Visible-light-driven CO<sub>2</sub> reduction with carbon nitride: enhancing the activity of ruthenium catalysts. *Angew. Chem. Int. Ed.* **2015**, *54*, 2406-2409.
- (14) Wang, M.; Chen, L.; Lau, T. C.; Robert, M. A Hybrid Co Quaterpyridine Complex/Carbon Nanotube Catalytic Material for CO<sub>2</sub> Reduction in Water. *Angew. Chem. Int. Ed.* **2018**, *57*, 7769-7773.
- (15) Wang, S.; Guan, B. Y.; Lu, Y.; Lou, X. W. D. Formation of hierarchical In<sub>2</sub>S<sub>3</sub>-CdIn<sub>2</sub>S<sub>4</sub> heterostructured nanotubes for efficient and stable visible light CO<sub>2</sub> reduction. *J. Am. Chem. Soc.* **2017**, *139*, 17305-17308.
- (16) Kuriki, R.; Ichibha, T.; Hongo, K.; Lu, D.; Maezono, R.; Kageyama, H.; Ishitani, O.; Oka, K.; Maeda, K. A Stable, Narrow-Gap Oxyfluoride Photocatalyst for Visible-Light Hydrogen Evolution and Carbon Dioxide Reduction. *J. Am. Chem. Soc.* **2018**, *140*, 6648-6655.
- (17) Yuan, S.; Feng, L.; Wang, K.; Pang, J.; Bosch, M.; Lollar, C.; Sun, Y.; Qin, J.; Yang, X.; Zhang, P. Stable Metal-Organic Frameworks: Design, Synthesis, and Applications. *Adv. Mater.* **2018**, 1704303.
- (18) Wu, X. Q.; Zhao, J.; Wu, Y. P.; Dong, W. W.; Li, D. S.; Li, J. R.; Zhang, Q. Ultrafine Pt Nanoparticles and Amorphous Nickel Supported on 3D Mesoporous Carbon Derived from Cu-Metal-Organic Framework for Efficient Methanol Oxidation and Nitrophenol Reduction. *ACS Appl. Mater. Interfaces* **2018**, *10*, 12740-12749.
- (19) Li, F. L.; Shao, Q.; Huang, X.; Lang, J. P. Nanoscale Trimetallic Metal-Organic Frameworks Enable Efficient Oxygen Evolution Electrocatalysis. *Angew. Chem. Int. Ed.* **2018**, *57*, 1888-1892.
- (20) Hao, J.; Xu, X.; Fei, H.; Li, L.; Yan, B. Functionalization of Metal-Organic Frameworks for Photoactive Materials. *Adv. Mater.* **2018**, *30*, 1705634.

- (21) Zhou, W.; Wu, Y. P.; Zhao, J.; Dong, W. W.; Qiao, X. Q.; Hou, D. F.; Bu, X.; Li, D. S. Efficient Gas-Sensing for Formaldehyde with 3D Hierarchical  $\text{Co}_3\text{O}_4$  Derived from  $\text{Co}_5$ -Based MOF Microcrystals. *Inorg. Chem.* **2017**, *56*, 14111-14117.
- (22) Zhang, F. M.; Dong, L. Z.; Qin, J. S.; Guan, W.; Liu, J.; Li, S. L.; Lu, M.; Lan, Y. Q.; Su, Z. M.; Zhou, H. C. Effect of imidazole arrangements on proton-conductivity in metal-organic frameworks. *J. Am. Chem. Soc.* **2017**, *139*, 6183-6189.
- (23) Wu, Y. P.; Zhou, W.; Zhao, J.; Dong, W. W.; Lan, Y. Q.; Li, D. S.; Sun, C.; Bu, X. Surfactant-Assisted Phase-Selective Synthesis of New Cobalt MOFs and Their Efficient Electrocatalytic Hydrogen Evolution Reaction. *Angew. Chem. Int. Ed.* **2017**, *56*, 13001-13005.
- (24) Trickett, C. A.; Helal, A.; Al-Maythaly, B. A.; Yamani, Z. H.; Cordova, K. E.; Yaghi, O. M. The chemistry of metal-organic frameworks for  $\text{CO}_2$  capture, regeneration and conversion. *Nat. Rev. Mater.* **2017**, *2*, 17045.
- (25) Li, X. X.; Shen, F. C.; Liu, J.; Li, S. L.; Dong, L. Z.; Fu, Q.; Su, Z. M.; Lan, Y. Q. A highly stable polyoxometalate-based metal-organic framework with an ABW zeolite-like structure. *Chem. Commun.* **2017**, *53*, 10054-10057.
- (26) Chen, Y. C.; Liu, J. L.; Wernsdorfer, W.; Liu, D.; Chibotaru, L. F.; Chen, X. M.; Tong, M. L. Hyperfine-Interaction-Driven Suppression of Quantum Tunneling at Zero Field in a Holmium (III) Single-Ion Magnet. *Angew. Chem. Int. Ed.* **2017**, *56*, 4996-5000.
- (27) Li, B.; Wen, H. M.; Cui, Y.; Zhou, W.; Qian, G.; Chen, B. Emerging multifunctional metal-organic framework materials. *Adv. Mater.* **2016**, *28*, 8819-8860.
- (28) Hou, B. L.; Tian, D.; Liu, J.; Dong, L. Z.; Li, S. L.; Li, D. S.; Lan, Y. Q. A water-stable metal-organic framework for highly sensitive and selective sensing of  $\text{Fe}^{3+}$  ion. *Inorg. Chem.* **2016**, *55*, 10580-10586.
- (29) Zhang, W.; Li, R.; Zhao, X.; Chen, Z.; Law, A. W.-K.; Zhou, K. A Cobalt-Based Metal-Organic Framework as Cocatalyst on  $\text{BiVO}_4$  Photoanode for Enhanced Photoelectrochemical Water Oxidation. *ChemSusChem* **2018**, *11*, 2710-2716.
- (30) Wu, R.; Wang, D. P.; Kumar, V.; Zhou, K.; Law, A. W. K.; Lee, P. S.; Lou, J.; Chen, Z. MOFs-derived copper sulfides embedded within porous carbon octahedra for electrochemical capacitor applications. *Chem. Commun.* **2015**, *51*, 3109-3112.
- (31) Renbing, W.; Xukun, Q.; Xianhong, R.; Hai, L.; Boluo, Y.; Kun, Z.; Jun, W.; Qingyu, Y.; X. Q. Feng.; Yi, L. Zeolitic imidazolate framework 67-derived high symmetric porous  $\text{Co}_3\text{O}_4$  hollow dodecahedra with highly enhanced lithium storage capability. *Small* **2014**, *10*, 1932-1938.
- (32) Sun, M.; Yan, S.; Sun, Y.; Yang, X.; Guo, Z.; Du, J.; Chen, D.; Chen, P.; Xing, H. Enhancement of visible-light-driven  $\text{CO}_2$  reduction performance using an amine-functionalized zirconium metal-organic framework. *Dalton Trans.* **2018**, *47*, 909-915.
- (33) Liu, J.; Fan, Y. Z.; Li, X.; Wei, Z.; Xu, Y. W.; Zhang, L.; Su, C.-Y. A porous rhodium (III)-porphyrin metal-organic framework as an efficient and selective photocatalyst for  $\text{CO}_2$  reduction. *Appl. Catal. B: Environ.* **2018**, *231*, 173-181.
- (34) Wang, S.; Yao, W.; Lin, J.; Ding, Z.; Wang, X. Cobalt imidazolate metal-organic frameworks photosplit  $\text{CO}_2$  under mild reaction conditions. *Angew. Chem. Int. Ed.* **2014**, *4*, 1034-1038.
- (35) Zhang, T.; Lin, W. Metal-organic frameworks for artificial photosynthesis and photocatalysis. *Chem. Soc. Rev.* **2014**, *43*, 5982-5993.
- (36) Chen, Y.; Wang, D.; Deng, X.; Li, Z. Metal-organic frameworks (MOFs) for photocatalytic  $\text{CO}_2$  reduction. *Catalysis Science & Technology* **2017**, *7*, 4893-4904.
- (37) Wang, C.; Xie, Z.; deKrafft, K. E.; Lin, W. Doping metal-organic frameworks for water oxidation, carbon dioxide reduction, and organic photocatalysis. *J. Am. Chem. Soc.* **2011**, *133*, 13445-13454.
- (38) Wang, X.; Wisser, F. M.; Canivet, J.; Fontecave, M.; Mellot-Draznieks, C. Immobilization of a Full Photosystem in the Large-Pore MIL-101 Metal-Organic Framework for  $\text{CO}_2$  reduction. *ChemSusChem* **2018**, *11*, 3315-3322.
- (39) Wang, D.; Huang, R.; Liu, W.; Sun, D.; Li, Z. Fe-based MOFs for photocatalytic  $\text{CO}_2$  reduction: role of coordination unsaturated sites and dual excitation pathways. *ACS Catal.* **2014**, *4*, 4254-4260.
- (40) Wang, Y.; Huang, N. Y.; Shen, J. Q.; Liao, P. Q.; Chen, X. M.; Zhang, J. P. Hydroxide Ligands Cooperate with Catalytic Centers in Metal-Organic Frameworks for Efficient Photocatalytic  $\text{CO}_2$  Reduction. *J. Am. Chem. Soc.* **2017**, *140*, 38-41.
- (41) Ye, L.; Gao, Y.; Cao, S.; Chen, H.; Yao, Y.; Hou, J.; Sun, L. Assembly of highly efficient photocatalytic  $\text{CO}_2$  conversion systems with ultrathin two-dimensional metal-organic framework nanosheets. *Appl. Catal. B: Environ.* **2018**, *227*, 54-60.
- (42) Zhao, J.; Wang, Q.; Sun, C.; Zheng, T.; Yan, L.; Li, M.; Shao, K.; Wang, X.; Su, Z. A hexanuclear cobalt metal-organic framework for efficient  $\text{CO}_2$  reduction under visible light. *J. Mater. Chem. A* **2017**, *5*, 12498-12505.
- (43) Chen, D.; Xing, H.; Wang, C.; Su, Z. Highly efficient visible-light-driven  $\text{CO}_2$  reduction to formate by a new anthracene-based zirconium MOF via dual catalytic routes. *J. Mater. Chem. A* **2016**, *4*, 2657-2662.
- (44) Yan, Z. H.; Du, M. H.; Liu, J.; Jin, S.; Wang, C.; Zhuang, G.-L.; Kong, X.-J.; Long, L.-S.; Zheng, L.-S. Photo-generated dinuclear  $\{\text{Eu}(\text{II})\}_2$  active sites for selective  $\text{CO}_2$  reduction in a photosensitizing metal-organic framework. *Nat. Commun.* **2018**, *9*, 3353.
- (45) Deng, X.; Albero, J.; Xu, L.; Garcia, H.; Li, Z. Construction of a Stable Ru-Re Hybrid System Based on Multifunctional MOF-253 for Efficient Photocatalytic  $\text{CO}_2$  Reduction. *Inorg. Chem.* **2018**, *57*, 8276-8286.
- (46) Zhang, S.; Li, L.; Zhao, S.; Sun, Z.; Luo, J. Construction of interpenetrated ruthenium metal-organic frameworks as stable photocatalysts for  $\text{CO}_2$  reduction. *Inorg. Chem.* **2015**, *54*, 8375-8379.
- (47) Chen, E. X.; Qiu, M.; Zhang, Y. F.; Zhu, Y. S.; Liu, L. Y.; Sun, Y. Y.; Bu, X.; Zhang, J.; Lin, Q. Acid and Base Resistant Zirconium Polyphenolate-Metalloporphyrin Scaffolds for Efficient  $\text{CO}_2$  Photoreduction. *Adv. Mater.* **2018**, *30*, 1704388.
- (48) Wen, L.; Zhao, J.; Lv, K.; Wu, Y.; Deng, K.; Leng, X.; Li, D. Visible-light-driven photocatalysts of metal-organic frameworks derived from multi-carboxylic acid and imidazole-based spacer. *Cryst. Growth Des.* **2012**, *12*, 1603-1612.
- (49) Wang, F.; Ke, X.; Zhao, J.; Deng, K.; Leng, X.; Tian, Z.; Wen, L.; Li, D. Six new metal-organic frameworks with multi-carboxylic acids and imidazole-based spacers: syntheses, structures and properties. *Dalton Trans.* **2011**, *40*, 11856-11865.
- (50) Cui, J. W.; Hou, S. X.; Li, Y. H.; Cui, G. H. A multifunctional Ni (II) coordination polymer: synthesis, crystal structure and applications as a luminescent sensor, electrochemical probe, and photocatalyst. *Dalton Trans.* **2017**, *46*, 16911-16924.
- (51) Wang, S.; Lin, J.; Wang, X. Semiconductor-redox catalysis promoted by metal-organic frameworks for  $\text{CO}_2$  reduction. *Phys. Chem. Chem. Phys.* **2014**, *16*, 14656-14660.
- (52) Li, R.; Zhang, W.; Zhou, K. Metal-Organic-Framework-Based Catalysts for Photoreduction of  $\text{CO}_2$ . *Adv. Mater.* **2018**, 1705512.
- (53) Dhakshinamoorthy, A.; Asiri, A. M.; Garcia, H. Metal-organic framework (MOF) compounds: photocatalysts for redox reactions and solar fuel production. *Angew. Chem. Int. Ed.* **2016**, *55*, 5414-5445.
- (54) Zhang, H.; Wei, J.; Dong, J.; Liu, G.; Shi, L.; An, P.; Zhao, G.; Kong, J.; Wang, X.; Meng, X. Efficient Visible-Light-Driven Carbon Dioxide Reduction by a Single-Atom Implanted Metal-Organic Framework. *Angew. Chem. Int. Ed.* **2016**, *55*, 14310-14314.

- 1 (55) Ouyang, T.; Huang, H. H.; Wang, J. W.; Zhong, D. C.; Lu, T.  
2 B. A Dinuclear Cobalt Cryptate as a Homogeneous Photocatalyst  
3 for Highly Selective and Efficient Visible-Light Driven CO<sub>2</sub>  
4 Reduction to CO in CH<sub>3</sub>CN/H<sub>2</sub>O Solution. *Angew. Chem. Int. Ed.*  
5 **2017**, *56*, 738-743.
- 6 (56) Kočí, K.; Obalová, L.; Matějová, L.; Plachá, D.; Lacný, Z.;  
7 Jirkovský, J.; Šolcová, O. Effect of TiO<sub>2</sub> particle size on the  
8 photocatalytic reduction of CO<sub>2</sub>. *Appl. Catal. B: Environ.* **2009**, *89*,  
9 494-502.
- 10 (57) Chen, X.; Zhou, Y.; Liu, Q.; Li, Z.; Liu, J.; Zou, Z. Ultrathin,  
11 single-crystal WO<sub>3</sub> nanosheets by two-dimensional oriented  
12 attachment toward enhanced photocatalytic reduction of CO<sub>2</sub> into  
13 hydrocarbon fuels under visible light. *ACS Appl. Mater. Interfaces*  
14 **2012**, *4*, 3372-3377.
- 15 (58) Liu, H.; Xu, C.; Li, D.; Jiang, H. L. Photocatalytic Hydrogen  
16 Production Coupled with Selective Benzylamine Oxidation over  
17 MOF Composites. *Angew. Chem. Int. Ed.* **2018**, *57*, 5379-5383.
- 18 (59) He, J.; Wang, J.; Chen, Y.; Zhang, J.; Duan, D.; Wang, Y.;  
19 Yan, Z. A dye-sensitized Pt@UiO-66(Zr) metal-organic  
20 framework for visible-light photocatalytic hydrogen production.  
21 *Chem. Commun.* **2014**, *50*, 7063-7066.
- 22 (60) Xie, S. L.; Liu, J.; Dong, L. Z.; Li, S. L.; Lan, Y. Q.; Su, Z. M.  
23 Hetero-metallic active sites coupled with strongly reductive  
24 polyoxometalate for selective photocatalytic CO<sub>2</sub>-to-CH<sub>4</sub>  
25 conversion in water. *Chem. Sci.* **2019**, *10*, 185-190.
- 
-

1  
2  
3  
4  
5  
6  
7  
8  
9  
10  
11  
12  
13  
14  
15  
16  
17  
18  
19  
20  
21  
22  
23  
24  
25  
26  
27  
28  
29  
30  
31  
32  
33  
34  
35  
36  
37  
38  
39  
40  
41  
42  
43  
44  
45  
46  
47  
48  
49  
50  
51  
52  
53  
54  
55  
56  
57  
58  
59  
60

---

**Table of contents (TOC)**

